Investigation into the High-Voltage Shutdown of the Oxygen Generation System Aboard the International Space Station

Joyce E. Carpenter[1]
Hamilton Sundstrand Space Systems International, Inc., Windsor Locks, CT 06096 USA

Gregory J. Gentry[2]
The Boeing Company, Houston, TX 77059 USA

Greg S. Diderich[3]
Jacobs Technology, Houston, TX 77058 USA

Robert J. Roy[4]
Hamilton Sundstrand Corporation, Windsor Locks, CT 06096 USA

Dr. John L. Golden[5]
The Boeing Company, Houston, TX 77059 USA

Steven P. VanKeuren[6]
Anadarko Industries L.L.C., Houston, TX 77058 USA

John W. Steele[7], Tony J. Rector[8], Jerome D. Varsik[9], Daniel J. Montefusco[10]
Hamilton Sundstrand Space Systems International, Inc., Windsor Locks, CT 06096 USA

Harold E. Cole[11] (retired)
Boeing Huntsville Laboratories, Huntsville, AL 35824 USA

Mark E. Wilson[12]
The Boeing Company, Houston, TX 77059 USA

and

Dr. Erica S. Worthy[13]
NASA Johnson Space Center, Houston, TX 77058 USA

[1] Staff Engineer, Space Systems, One Hamilton Road, M/S 1A2-W66, non-Member.
[2] ISS ECLS Technical Lead, 13100 Space Center Blvd., MC HB2-40, Senior AIAA Member.
[3] Subsystem Manager, ISS ECLS, 2101 NASA Parkway, M/S EC6, non-Member.
[4] Principal Engineer, Space Systems, One Hamilton Road, M/S 1A2-W66, Senior AIAA Member.
[5] Technical Fellow, 13100 Space Center Blvd., MC HB3-20, non-Member.
[6] ISS ECLS Systems Engineer, 17625 El Camino Real 410, non-Member.
[7] Fellow, Materials Engineering, Space Systems, One Hamilton Road, M/S 1A2-W62, Professional Member.
[8] Staff Materials Engineer, Space Systems, One Hamilton Road, M/S 1A2-W66, Senior AIAA Member.
[9] Engineering Manager, Space Systems, One Hamilton Road, M/S 1A2-W66, Senior AIAA Member.
[10] Staff Engineer, Space Systems, One Hamilton Road, 1A2-W66, non-Member.
[11] Chemist, Huntsville Laboratory (retired), Water Analyses, 499 Boeing Blvd., non-Member.
[12] Associate Technical Fellow, Research & Technology, 13100 Space Center Blvd., MC HB3-20, Senior AIAA Member.
[13] Materials Research Engineer, Materials and Processes Branch, Structural Engineering Division, 2101 NASA Parkway, non-Member.

Abstract

The Oxygen Generation System (OGS) Hydrogen Dome Assembly Orbital Replacement Unit (ORU) serial number 00001 suffered a cell high-voltage shutdown on July 5, 2010. The Hydrogen Dome Assembly ORU was removed and replaced with the on-board spare ORU serial number 00002 to maintain OGS operation. The Hydrogen Dome Assembly ORU was returned from ISS on STS-133/ULF-5 in March 2011 with test, teardown and evaluation (TT&E) and failure analysis to follow. The purpose of this paper is to summarize the results of the failure analysis.

Keywords

Oxygen Generation System, Electrolysis Cell Stack, Hydrogen Dome Assembly Orbital Replacement Unit

Nomenclature

asf	amps/square foot, unit of current density
µS/cm	micro-Siemens/centimeter, unit of conductivity
ppm	parts per million, unit of concentration
mg/L	milligrams/liter, unit of concentration
Vdc	volts, direct current, unit of potential difference

I. Introduction

Oxygen Generation System (OGS) Hydrogen Orbital Replacement Unit (Hydrogen ORU) serial number (S/N) 00001 was built with Electrolysis Cell Stack Assembly (cell stack) S/N0003 in 2003. The OGS was launched in 2006, made operational in 2007, and operated 231 days on-orbit as commanded until it experienced a cell stack high-voltage shutdown on July 5, 2010. The fast shutdown of the OGS occurred when Cell 27 of the cell stack prematurely exceeded its high limit of 3.0 volts while operating at the 100% production rate. Cell life is expected to exceed the five-year life of the Hydrogen ORU. It was also observed that Cell 18 was shadowing Cell 27 but had not quite reached the 3.0 volt high limit. All other cells exhibited some increase in voltage as well. The Hydrogen ORU S/N00001 was removed and replaced with the on-board spare ORU S/N00002 to maintain OGS operation. The Hydrogen ORU was returned from the International Space Station (ISS) on STS-133/ULF-5 in March 2011 with subsequent test, teardown and evaluation (TT&E) and failure analysis (F/A) at Hamilton Sundstrand in Windsor Locks, CT.

This paper begins with a description of the Oxygen Generation System (OGS), including a description of the Electrolysis Cell Stack Assembly (cell stack) hardware and electrolysis process, and on-orbit events which preceeded the OGS high-voltage shutdown. A high-level view of the fault tree and a summary of the evidence collected are presented. The physical and mechanistic root causes are then discussed, followed by a description of the on-orbit mitigation currently in place.

A. Oxygen Generation System

The Oxygen Generation System (OGS) consists of the Oxygen Generation Assembly (OGA), the Power Supply Module (PSM), the Avionics Air Assembly (AAA) Fan and smoke detector. Figure 1 shows a simplified schematic for the OGA. The black box indicates the boundary for the Hydrogen ORU. The OGS is designed to generate oxygen at a maximum rate of 5.4 kg/day (12 lb_m/day) when operated on day/night orbital cycles, and also at a selectable rate between 2.3 and 9.2 kg/day (5.1 and 20.4 lb_m/day) when operated continuously. The product oxygen meets quality specifications for temperature, free water, dewpoint, and hydrogen content.

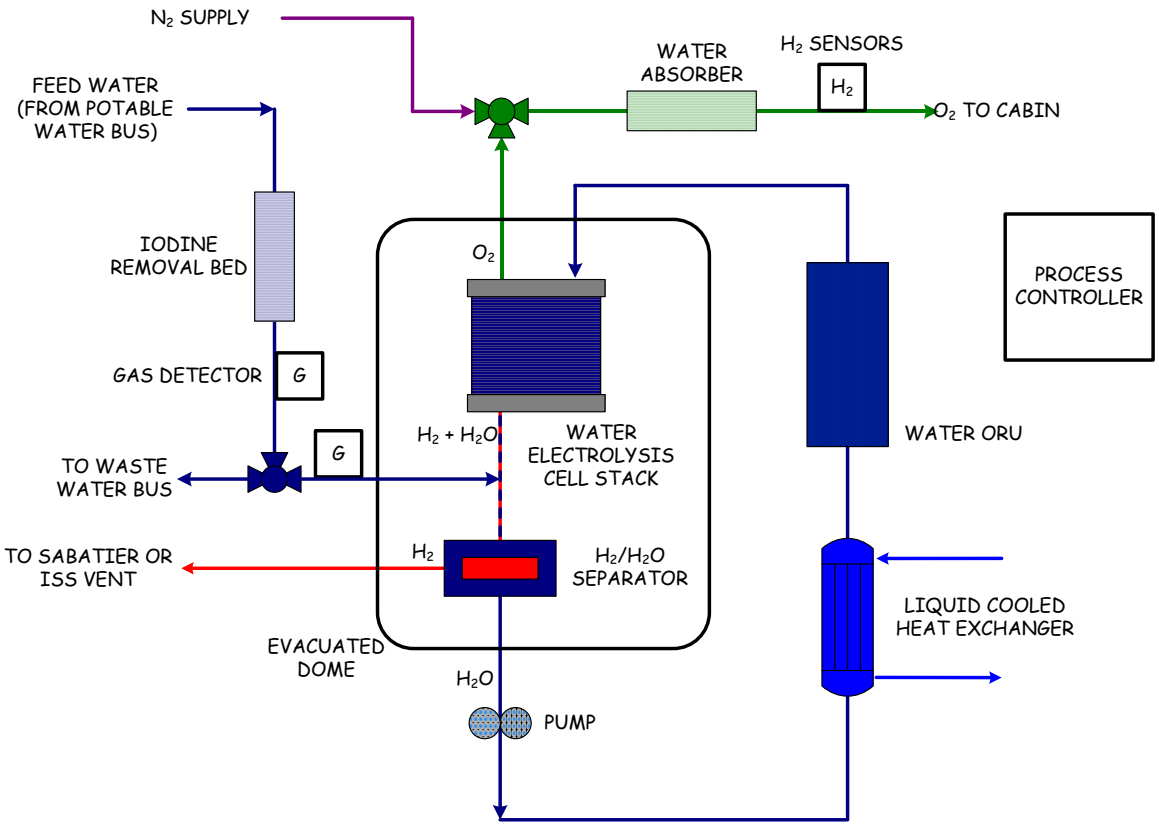

Figure 1. Oxygen Generation Assembly Simplified Schematic.

B. Electrolysis Cell Stack

In its simpliest description, an electrolysis cell stack consists of repeating sets of 'cells'. See Table 1 for a list of cell components and their function. For simplicity, in-cell sealing and load maintaining parts are omitted. The cells are layered between a base plate at the bottom of the stack and a terminating separator, positive terminal, insulator plate and compression plate at the top of the stack. These are followed by associated compressive hardware which maintains proper preload on the cell stack creating a sealed and electrically-conductive unit.

Table 1. Cell Assembly Building Block

Component	Function
Hydrogen separator plate	Separation of the hydrogen/water cavity of one cell from the oxygen cavity of the adjacent cell.
Water transport plate	Distribution of water across the MEA, removal of hydrogen and water at cell exit.
Membrane & Electrode Assembly (MEA)	Electrolysis of water. The MEA consists of Nafion® membrane and catalyst layers applied to either side of the membrane which form the electrodes.
Oxygen transport plate	Collection and flow passage for oxygen removal from cell; also serves as nitrogen purge pathway.
Oxygen separator plate	Separation of the oxygen cavity from the in-cell compression assembly.

In the electrolysis process, current flow between positive and negative electrodes is accomplished by the movement of ionic species. Since pure water does not provide an abundance of ionic species, an electrolyte must be present for the water to support water electrolysis. A separator diaphragm is also required to prevent the product

Nafion® - Registered trademark of E. I. du Pont de Nemours and Company

gases from mixing. The separator must be permeable to the water/electrolyte, but have limited permeability to the product gases. The proton-exchange membrane (PEM) water electrolysis cell produced by Hamilton Sundstrand uses a tough plastic sheet of a sulfonated perfluorinated polymer, manufactured by DuPont under the trade name of Nafion.

Nafion membrane is conductive to proton transport due to its absorption of liquid water. Proton conductivity, which defines how readily protons can migrate through the membrane, is strongly dependent on the structure of the membrane as well as its water content. There are two water environments defined in Nafion: surface water, which is near the pore surface along the array of sulfonate ($-SO_3^-$) groups, and bulk water which is contained in the middle region of the pore. Factors that determine membrane water content include the equivalent weight of the polymer, the nature of the cation coordinated with the sulfonate group (for virgin Nafion, the coordinate cation is the hydrogen ion, or proton), and the method of pretreatment of the membrane. Note that Nafion membrane is vulnerable to cation contamination due to the sulfonic acid end group's high affinity for foreign cations. In fact, most cations have a higher affinity for sulfonic acid than H^+. Exchange of cations causes changes to the bulk properties of the membrane; specifically, the ionic conductivity decreases proportionately to the cation ionic charge, and the water content decreases as less water is coordinated.

C. Liquid Cathode Feed Water Electrolysis Cell Stack

Water may be fed to the electrolysis cell either as a liquid or vapor to either the anode or cathode cavity. System design considerations define the water feed method that is most appropriate for the application being considered. The cell stack for the OGS is a liquid cathode feed configuration. Figure 2 illustrates the electrochemical reactions occurring in a single liquid cathode feed water electrolysis cell. In the liquid cathode feed mode of operation, process water is fed to the cathode (hydrogen side) of the electrolysis cell. Liquid water, under a physical and chemical potential gradient, diffuses through the polymer electrolyte to the anode (oxygen side), where it is dissociated into oxygen, hydrogen ions, or protons, and electrons. Hydrated protons migrate through the membrane from the anode to the cathode, and electro-osmotically drag water away from the anode. This condition effectively maintains the anode side of the membrane (anolyte) at low water content; thus, the exiting oxygen gas is free of liquid water. Due to the elevated water concentration gradient across the membrane, the polymer electrolyte ohmic resistance is moderately affected by cell current density, resulting in higher cell polarization (higher voltage) as compared to a liquid anode feed cell operating at the same conditions. The operational current density for liquid cathode feed cells is limited to prevent complete anolyte dry out and potential cell damage, resulting in an increase in the number of cells required for a specific gas output. Oxygen and hydrogen are generated in a stoichiometric ratio at a rate proportional to the cell current. Excess water is delivered to the cathode cavity such that the heat generated from the cell reactions is transported and rejected to an external heat sink.

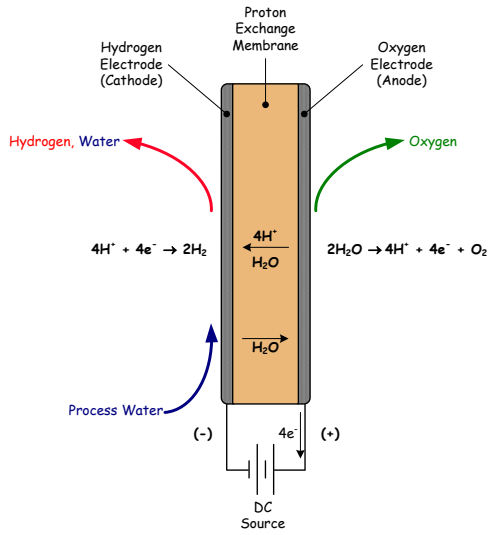

Figure 2. Liquid Cathode Feed Water Electrolysis Cell.

II. On-Orbit Anomalies Preceding OGS High-Voltage Fault Shutdown

Preceeding the Hydrogen ORU high-voltage fault, several anomalies occurred on-orbit. Figure 3 shows a timeline of events pre- and post- ORU fault.

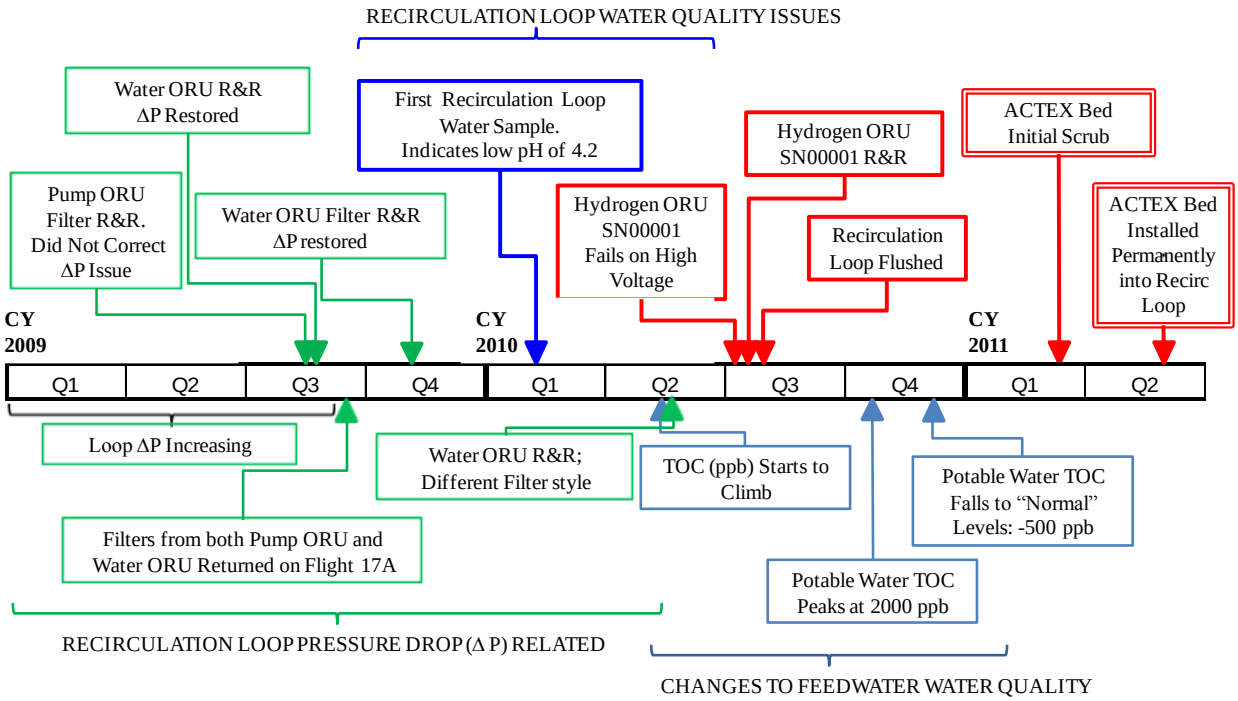

Figure 3. Timeline of Events On-Orbit Before and After Hydrogen ORU S/N00001 Fault.

1. High Differential Pressure (ΔP) Drop in the Recirculation Loop

The differential pressure sensor across the recirculation loop pump showed increasing pressure drop indicative of a flow blockage somewhere in the recirculation loop. Figure 4 illustrates several exponential curves with increasing slopes. Early troubleshooting of the rising ΔP assumed that the *most likely* cause was the Pump ORU inlet filter. Initially it was thought that the source of particulate clogging the filter was catalyst material shed from the cell stack. The Pump ORU inlet filter was replaced August 18, 2009 with no improvement in the loop pressure drop. The next most likely component was a filter in the Water ORU Flow Measurement Zone. In this case it was thought that the source of particulate clogging the filter was from the gears in the OGS recirculation loop pump. This second attempt to restore pressure drop called for the replacement of the Water ORU with an on-orbit spare. The ORU was replaced August 22, 2009 and pump ΔP returned to normal (1st filter). This was short-lived as the increasing ΔP returned at a more rapid rate. Two additional water inlet filters were replaced in the Water ORU with similar, short-term, successful results (2nd & 3rd filters). It was noted, however, that each additional filter replacement saw faster filter loading. The inlet water filter in the Water ORU was ultimately replaced with an alternate design (4th filter) that provided approximately four times as much effective filter area. Figure 4 shows the filters' pressure rise graphically and indicates (▲) Hydrogen ORU S/N00001's high-voltage fault approximately two months after the last filter replacement.

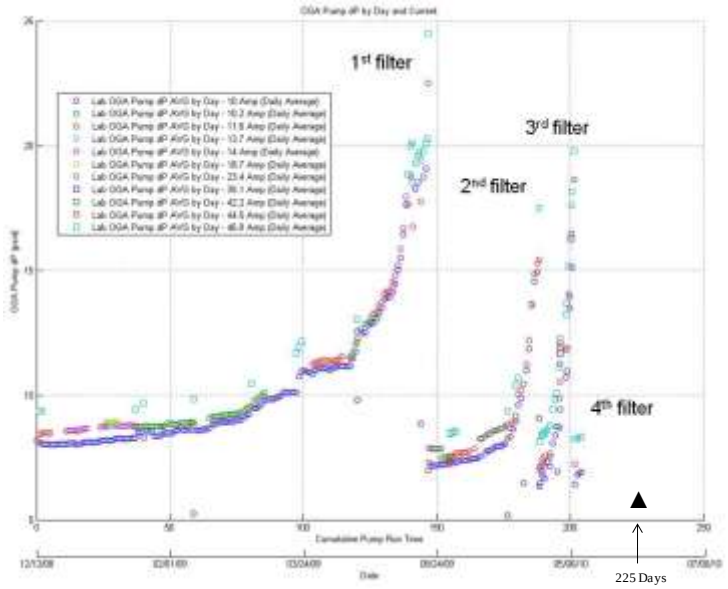

Figure 4. OGS Recirculation Loop Differential Pressure (DP7131) by Day (0-250 days).

2. Recirculation Loop Water Quality

A water sample was drawn on February 5, 2010 and returned from orbit on STS130 to aid in understanding and locating the source of debris blocking the Water ORU filters. The pH of the water was low (pH = 4.19), and there were significant levels of metals both in solution as ionic species and as particulate. See summary contained in Table 2. To better understand the results of this and subsequent water analyses, various activities were conducted such as single cell land-based testing, the development of a "Bleed and Feed" on-orbit procedure, and the development of an on-orbit hand-held conductivity sensor and conductivity strip testing.

Table 2. OGS Recirculation Loop Water Sample Collected February 5, 2010

Particulate information	
Particle size 0-50 micron	47,100 particles per 100 ml
pH	4.19
Conductivity	34.5 µS/cm
Anions (dissolved)	
Fluoride	1.15 mg/L
Sulfate	4.15 mg/L
Carbon Analysis	
TC	2.93 ppm
TIC	<1.0 ppm
TOC	2.93 ppm
MetalsAnalysis	
Sum (19 Elements analyzed)	1.687 ppm Total
Sum (19 Elements analyzed)	0.142 ppm Dissolved

3. DMSD Increase in OGA feed water

In 2010, an unexpected rise in the organic compound dimethylsilanediol (DMSD) was observed in the output of the Water Processor Assembly (WPA). Normal Total Organic Carbon Analyzer (TOCA) readings were well below the minimum detectable levels of 475 ppb. In June 2010 a sudden increase in TOC was observed, peaking around 2000 ppb. By October 26, 2010 this event had subsided and the TOC levels rapidly decayed back to baseline levels. A separate ground-test program of a single electrolysis cell challenged with DMSD was conducted; the results indicated DMSD was likely not a contributing factor in the failure of the Hydrogen ORU, but further study is warranted as extended dormancy period indicated a loss of electrolysis capability at cell stack re-start.

III. Teardown and Failure Investigation

The cell stack portion of the test, teardown and evaluation (TT&E) was conducted from March 23 until July 8, 2011. From March 22 to March 31, Boeing and NASA were on-site at Hamilton Sundstrand to support the Hydrogen ORU and cell stack disassembly. Initially during the cell stack disassembly, only Cells 28, 27 and 26 were removed. As the investigation proceeded, the team felt confident in proceeding further without disruption of evidence. By the end of the failure investigation, the entire stack was disassembled in either units of single cell assemblies (16 cells) or triplet cell assemblies (four sets). Each step was documented with pictures and notes, with water and swab samples collected at various steps. The failure investigation began with the TT&E and continued through October 2011.

The initial fault tree had two main branches: increased resistance in the cell stack and/or issues with the electrical hardware/measurement issues in the Hydrogen Dome ORU, associated rack wiring and/or process controller. A high-level view of the fault tree is shown in Figure 5.

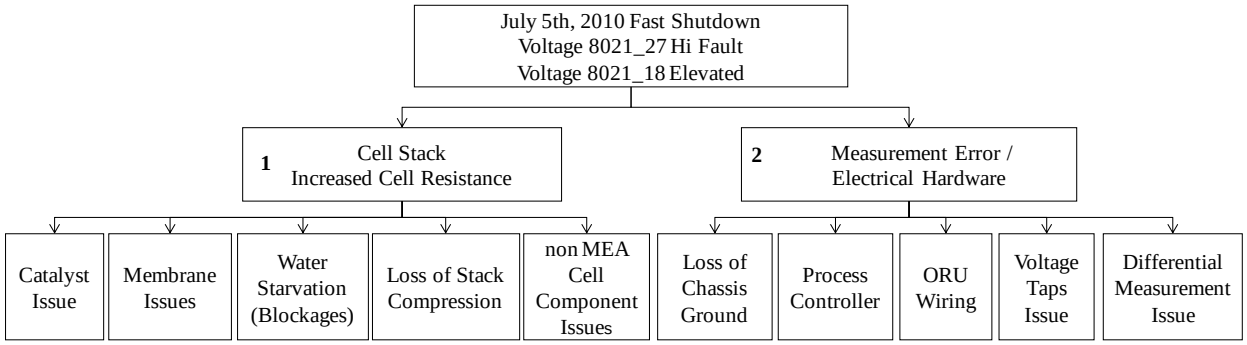

Figure 5. High-Level Breakdown of Fault Tree.

Prior to the TT&E commencing in March 2011, the leading theory for increased cell resistance was blockage of water delivery to the MEAs, either physical blockage of the water inlet passages of the hydrogen frame and screen assemblies or at the surface of the MEAs, based on observations from the TT&E of the inlet screen filter to the Water ORU S/N00001. This filter had been removed from the Water ORU and returned from orbit for TT&E due to the excessive rise in pressure drop. Roughly 2/3 of the filter openings were blocked with a hard/brittle extrudate on the downstream side of the filter. Composition of the extrudate was determined, and the source material was thought to derive from the Pump ORU.

Early in the TT&E and failure investigation, cell resistance measurement error was eliminated. If a failure had occurred within the controller on a single cell monitor input, it would have affected the reading on both the failed and adjacent cell reading. In the case of the cell voltage issue seen on-orbit, the two cells which showed atypical readings were not adjacent. The readings on the cells adjacent to the two in question were nominal. This issue was indicative of an actual change in the cell voltages and not a controller failure. When S/N00001 Hydrogen ORU was replaced with S/N00002, the OGA was powered on and operated normally. This further indicated that the issue was with the H2 ORU itself, and not the rack resident harnessing and controller.

During the TT&E all cell stack and Hydrogen ORU harnessing were verified to be electrically acceptable. The harnesses were tested by various methods (insulation resistance, dielectric and /or continuity) to verify that the harnesses were within acceptable limits. As mentioned above, the failure mode was indicative of neither a harness issue nor a controller issue. At this point, the failure investigation focused on cell stack sources of increased cell resistance.

The compressive load on the stack was as expected eliminating overall load loss as a cause of high resistance. Water and swab samples of the hardware were taken at multiple locations. Microbial and fungal causes were eliminated through analysis of the water and swab samples. Fourier transform infrared spectroscopy (FTIR) and scanning electron microscopy/energy dispersive X-ray spectroscopy (SEM/EDS) analyses did not identify constituents which could have increased the hydrophobicity of the MEA. Through the swab and water samples, as well as analysis of the MEAs and non-MEA cell components, fault tree branches related to microbial, fungal, and organic contaminants were eliminated. No evidence of blockages in the water passages were observed.

The top two cells were removed for destructive analysis. Cell 28, a nominally performing cell assembly, and Cell 27, a failed cell, were disassembled and visually inspected. The hydrogen and oxygen transport plates showed no evidence of blockages. The wet MEA surfaces did not appear hydrophobic nor were there deposits/precipitates on the surface. Visually the catalyst layers appeared well-adhered. From both Cell 28 and Cell 27 MEAs, samples were cut and sent for examination by SEM/EDS. The catalyst layers for both MEAs had only incidental levels of cations. Cross-sections of the water/hydrogen and oxygen transfer plates were also examined by SEM and did not reveal contamination or blockages. At magnification, however, evidence of corrosion was clearly seen in the water/hydrogen transport plates. In all, fourteen cell assemblies of the twenty-eight total were taken apart and visually inspected. No changes in appearance such as dryout of the MEAs, no occluding surface deposits, catalyst layer delamination, or hydrophobicity were seen. One cell had evidence of a single FOD particle, later determined to likely originate in equipment used in the part storage prior to cell assembly, but which did not contribute to the failure. These fourteen cells were destructively analyzed for contaminants. Significant metal contamination was found in the cell membrane, with the metals representative of loop and cell hardware.

Additionally, a number of tests on either single cell assemblies or triplet cell assemblies were conducted in the laboratory. The triplet of Cells 17,18 and 19 was run in a laboratory test rig, and failed to support operation at 100%, duplicating the on-orbit failure.

IV. Root Causes

A. Increased Cell Resistance Through Membrane Chemical Degradation

The resistance of an electrochemical cell includes ionic and electronic contributions that ultimately establish the operating voltage of the cell. Ionic resistance is a measure of how efficiently the water electrolysis cell membrane transports protons across the membrane, whereas electronic resistance provides an indication of how well the electrodes and current collectors conduct and transport electrons through the cell support hardware. The extensive testing conducted over the course of this failure investigation essentially identified the cell membrane as the source of increased resistance due to the reduction of proton exchange sites within the membrane and a reduction in the membrane water content. Analytical testing of cell membranes removed from this cell stack, along with the results of single cell testing that was conducted independently of the flight hardware investigation, isolated cation adsorption by the membrane as the root cause for reduced proton conduction and membrane water content. These factors adversely impacted the ohmic and concentration overpotential of the water electrolysis cells in the stack assembly and ultimately led to the fast shutdown of the Hydrogen ORU in July 2010.

There was significant evidence supporting cationic contamination of the membrane adversely impacting the cell resistance. As can be seen in Figure 6, the resistance of all the cells in the cell stack assembly increased, with the largest gains observed in Cell 27, which had triggered the fast shutdown of the Hydrogen ORU, and Cell 18, which exhibited the next highest voltage in the cell stack.

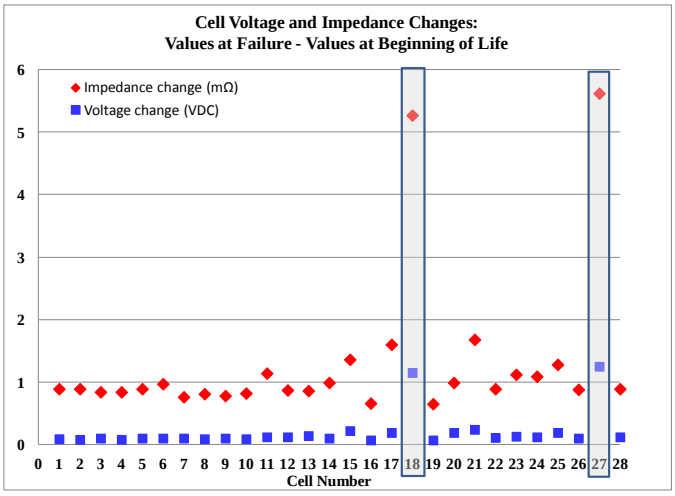

Figure 6. Changes in Cell Impedance and Voltage.

The results of the microprobe analysis of select membranes conducted by the United Technologies Research Center (UTRC) and the aqua regia digestion of a wide cross-section of cell membranes (14 total) by UTC Power and Hamilton Sundstrand revealed significant cationic contamination. Figure 7 shows multiple membrane cross-sections cut from the MEA corresponding to the flow path of water transport plate from water inlet to hydrogen/water exit. Location and intensity of each element are indicated by intensity of color in the figure. For the same elements shown in Figure 7, Table 3 contains the milligrams of contamination (digested sample result scaled to a whole MEA). These analytical results provided the first insight into the degree of cationic contamination of the cell membranes.

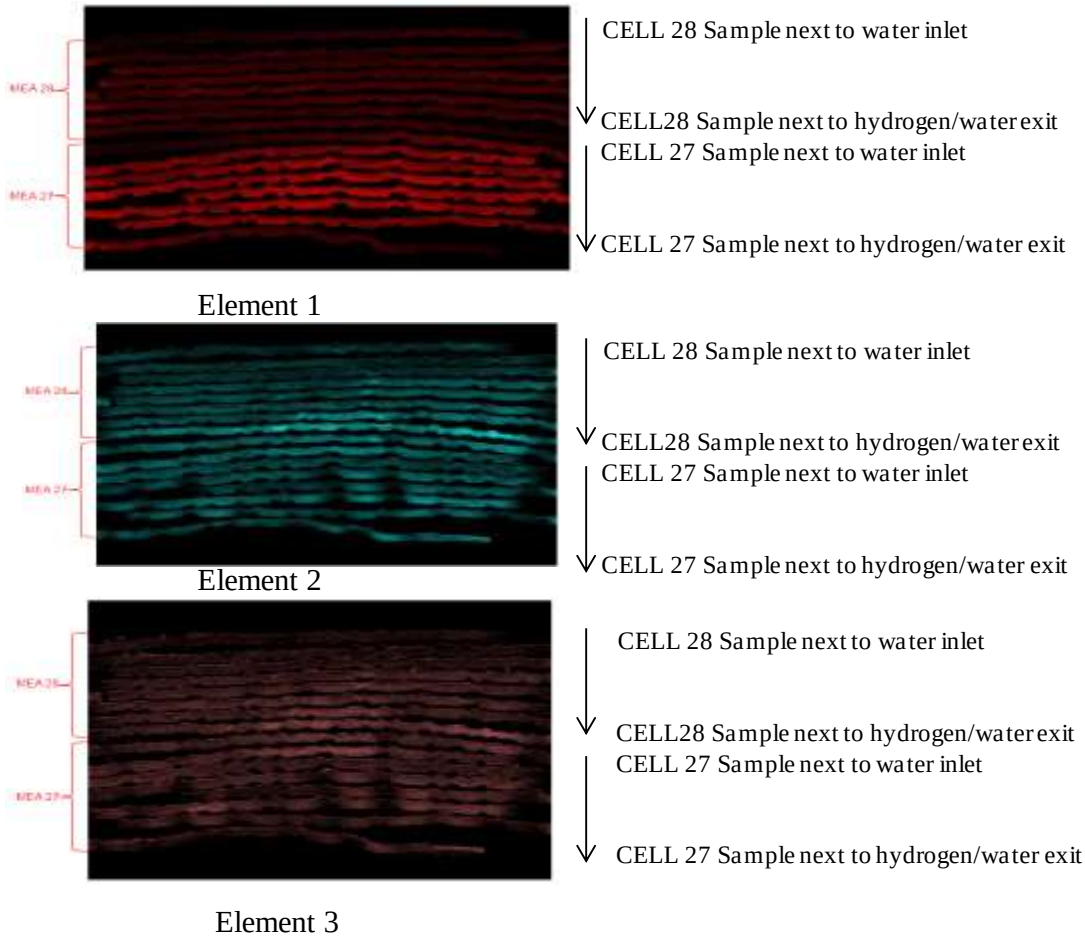

Figure 7. SEM/EDS MEA Cross-Sections for Three Elements.

Table 3. Aqua Regia MEA Digestion Results

Species	Milligrams/MEA (14 Cells)	
	Range	Average
Element 1	29-72	49
Element 2	9-16	13
Element 3	3-6	4

1. Reduced Water Content

Chemical degradation of the cell membrane due to cationic contamination reduces the water content of the membrane, adversely impacting both the cell resistance (discussed above) and the water transport characteristics of the membrane. With a liquid cathode feed water electrolyzer, water must transport from the bulk fluid stream on the cathode side of the cell to the anode for electrolysis to occur. As the diffusion coefficient is strongly dependent on the water content of the membrane, cationic contamination retards the water transport characteristics of the membrane significantly increasing the concentration overpotential of the water electrolysis cell. This characteristic is apparent in the cell polarization curve where the plot of cell voltage versus current density becomes asymptotic at the cell's limiting current density. As the water content of the cell is reduced due to cationic contamination, the polarization curve and the cell's limiting current density shift to the left due to the inability of the cell membrane to maintain the water transport rate at a specific oxygen output level. The asymptotic change in the cell's limiting current density is evident in the steep increases in the cell voltages observed just prior and up to the point of the fast shutdown of the Hydrogen ORU as seen in Figure 8.

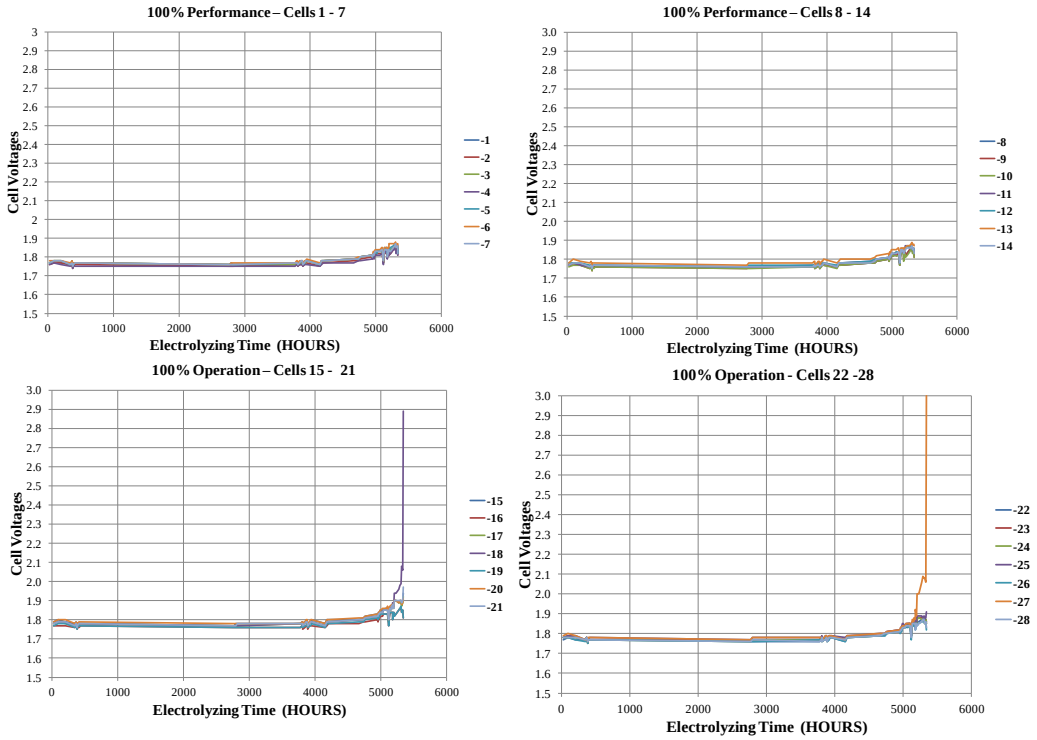

Figure 8. On-Orbit Performance Data at 100% Operation for Electrolysis Cell Stack S/N00003.

2. Reduced Proton Exchange Sites

Testing of Cells 17, 18 and 19 in the laboratory showed stable operation at low oxygen production rates (25%); however, as the production rate was increased to 50% or 100%, Cell 18 triggered an automatic shutdown of the test article and test system due to rapid voltage rise. The polarization curves for the triplet of Cells 17, 18 and 19 is included in Figures 9, and provides evidence of reduced membrane water content and its adverse impact on the concentration overpotential and limiting current density of an operational water electrolysis cell.

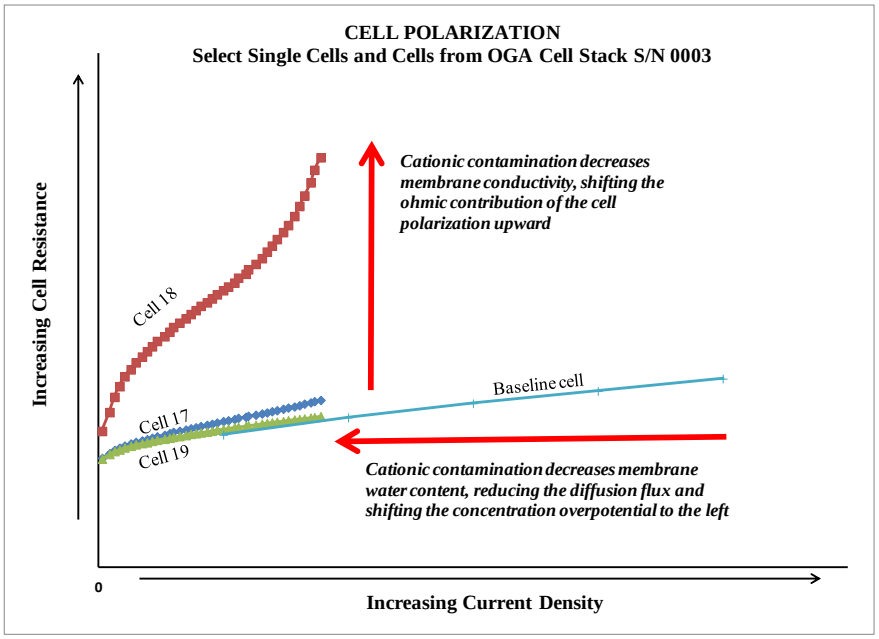

Figure 9. Polarization Curve – Cells 17, 18, 19 from Hydrogen ORU and Baseline MEA.

B. Mechanistic Causes of the Cationic Contamination

Two mechanistic causes for cationic contamination of the cell stack were identified during this failure investigation – corrosion of cell and system hardware due to the low pH of the recirculating water loop, and shunt currents present in the cell stack due to increased conductivity of the process water due to increased ionic contaminants that resulted in the electrochemical dissolution of the terminating separator sheet at the cell stack anode.

1. Recirculating Water Loop pH

The low pH of the recirculating water loop was the result of degradation of the Nafion membrane, which releases low levels of hydrofluoric and sulfuric acids as well as carbon dioxide. As is seen in Table 4, the pH of the water in the recirculation loop on-orbit was 4.19. The local pH at the MEA-to-water transport plate interface would likely be lower as the hydrofluoric and sulfuric acids are released by the membrane into the bulk fluid stream. This phenomenon was replicated in ground testing of two single-cell assemblies which produced similar results of low pH water and elevated fluoride and sulfate concentrations in the recirculating loop water. Materials for use in the OGS were selected assuming the process loop would be maintained at a neutral pH of 7. However, when the acid concentration in the loop continued to increase, materials used in the construction of the cell stack cathode cavity as well as materials used in recirculation loop began to corrode, releasing cations into the process water loop which were subsequently adsorbed by the proton-exchange membrane.

As the pH of the loop began to decrease and the concentration of ions in the loop began to increase, the conductivity of the water also began to increase. As a result, the shunt currents increased between the terminating separator and closest hydrogen separator sheets, to the cell stack compression plate, accelerating the electrochemical dissolution rate of the separator sheets. The metal cations introduced into the process water loop increased. Based on the complex chemistry of the metals at varying pH levels, some species remained in solution and exchanged into the cell membrane whereas some remained as a complex containing oxygen and fluoride as witnessed during the filter evaluation.

2. Accelerated Polymer Degradation through Attack by Reactive Species

Nafion membrane is made conductive by its absorption of water. However, the water also allows dissolution of the product hydrogen and oxygen into the membrane thereby permitting its transport via a diffusion mechanism (from an area of high concentration to one of low concentration). The diffusion of the product oxygen from the cell anode cavity to the cell cathode results in degradation of the membrane, due to attack by hydroxyl and peroxyl radical species that form from the reaction of oxygen with hydrogen on the catalytic hydrogen electrode, and to a lesser extent, by oxygen. These oxidative species attack the end groups of the polymer, releasing acid species (hydrofluoric and sulfuric acids and carbon dioxide) and perfluorocarbon compounds. As the concentration of the acids increases in the process water loop, the pH decreases and corrosion of metallic hardware begins, releasing cations into the loop. These cations exchange into the membrane adversely impacting its resistance and water content. Unfortunately, certain transition elements serve as catalysts in a Fenton's reaction, accelerating membrane degradation and the formation and release of hydroxyl and peroxyl radicals. A feedback loop is subsequently established where increasing acid concentration in the loop results in increased corrosive attack, increased cationic contamination of the membrane and accelerated membrane degradation. Absent modifications to the chemistry in the process loop, such as removal of the generated acid, the process proceeds essentially unchecked resulting in rapid poisoning of the cell membrane and its deleterious effects on cell performance.

Figure 10 illustrates the Membrane Chemical Degradation branch of the fault tree and pictorially summarizes the mechanistic causes of the electrolysis cell stack increased cell resistance.

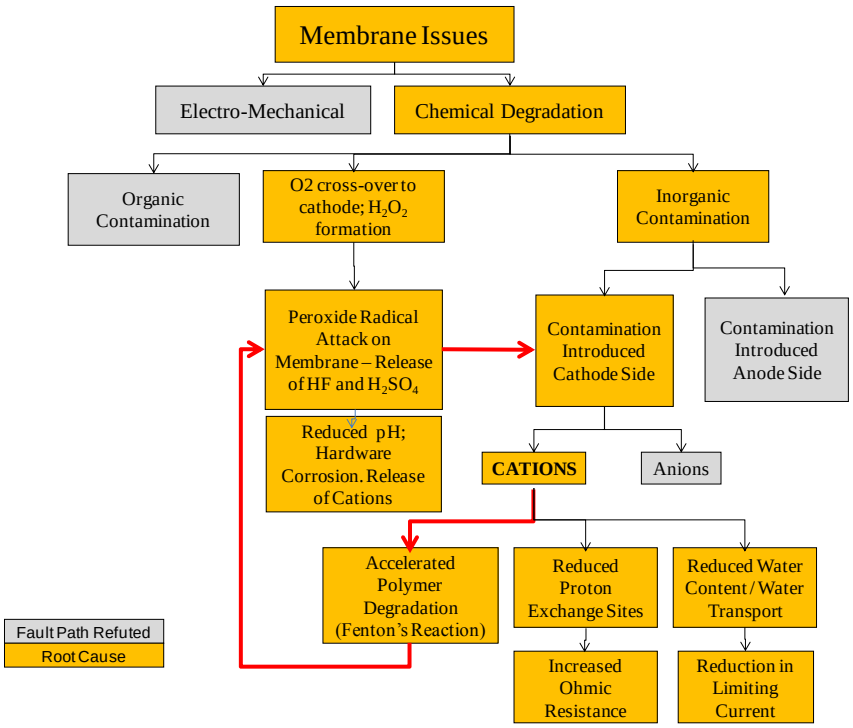

Figure 10. Fault Tree Branch for Membrane: Chemical Degradation Branch.

V. On-orbit Mitigation

Although the generation of hydrofluoric acid (fluoride) within the cell stack is tied to the fundamental design and operation of the membrane, and cannot be avoided, accumulation of the fluoride and the negative effects of low pH can be minimized with the installation of a mixed resin deionization bed within the OGS water recirculation loop.

The current on-orbit solution is the use of the mixed resin Deionizing (DI) Bed. Table 4 shows a shortened list of the recirculation loop water quality before the DI Bed installation (2010 day 300 and 2011 day 39), after a few hours with the DI Bed installed (day 64), and another sample taken after approximately 2 months of operation (day 197). The DI Bed bed provides improved water quality with respect to pH, conductivity and fluoride concentration.

Table 4. Summary of Recirculation Loop Water Quality w/ DI Bed

Sample Year/Day	pH	Conductivity (µS/cm)	Fluoride (ppm)	Comments
2010/300	4.6	14.67	0.27	S/N00002 Hydrogen ORU installed with 12.1 day cumulative run time
2011/039	4.36	19.5	0.31	
2011/064	5.37	1.8	<0.03	Several hours after DI Bed installed
2011/197	5.51	1.71	<0.03	Two months after DI Bed installed

The DI Bed used, the ACTEX, was originally designed for use in the potable water loop to remove iodine, and was also used in the EMU recirculation loop. When the low OGS recirculation loop pH was identified, a spare ACTEX bed was available and flown to ISS and installed. The DI Bed does add significant pressure drop to the recirculation loop as well as potentially having a shorter than desired life. Considerations for a deionization bed designed specifically for use in the OGS recirculation loop should include: water sampling capability, easy access via the front of the rack, updates to contaminant model (if available) and minimal pressure drop. Integrating water

sampling capability with the deionization bed at the front of the rack will facilitate sampling and bed change-out. Minimizing the pressure drop of the deionization bed would limit the burden on the pump and allow for any unanticipated increase in loop pressure drop over time.

VI. Conclusions

On July 5, 2010 the Hydrogen Dome Assembly ORU S/N00001 experienced a high-voltage fault on the electrolysis cell stack's Cell 27 and an elevated voltage warning on Cell 18. The Hydrogen Dome Assembly ORU was returned from ISS on STS-133/ULF-5 in March 2011 with subsequent TT&E. Extensive investigation into the failure was conducted from March 2011 through December 2011.

The failure was due to chemical degradation of the cell membranes during nominal electrolysis, resulting in the formation of degradation byproducts – specifically hydrofluoric acid and, to a much lesser extent, sulfuric acid. These acid constituents accumulated over time in the OGS recirculating water loop, lowering the loop pH to the point of corroding metallic hardware in both the cell stack and balance of plant hardware. The corrosion products accumulated in the recirculation loop fluid with impacts in four main areas:

1. The cationic corrosion by-products exchanged into the Nafion membrane, displacing the proton coordinated with the sulfonyl end group of the membrane and increasing the resistance to proton transfer across the membrane. The result is an upward shift in cell voltage for a given oxygen production rate.
2. As the membrane continued to be poisoned by the cationic corrosion by-products, the water content of the membrane was reduced, increasing the resistance to proton transfer across the membrane and reducing the diffusional flux of water from the bulk fluid stream of the recirculating water loop to the cell anode where the electrolysis reaction is initiated. The reduction in diffusional flux resulted in cell operation where water was consumed faster than it could be replenished by the normal transport process, resulting in water starvation at the cell anode and a rapid growth in the voltage degradation rate.
3. The adsorbed cations in the membrane functioned as catalysts for Fenton's Reaction, accelerating the rate of membrane degradation by increased production of oxidative species which in turn accelerated the release of hydrofluoric and sulfuric acids by the membrane, further dropping the pH of the recirculating water loop.
4. The introduction of acids and cationic corrosion by-products, absent a mechanism for their removal, increased the conductivity of the water in the recirculation loop. As the fluid conductivity increased, the shunt current present between the terminating separator at the cell stack anode and the compression plate of the electrolysis cell stack, which is at cathodic potential, increased, resulting in significant corrosion of the terminating separator and, to a lesser extent, the hydrogen separator sheets of Cell 28 and 27. These additional corrosion by-products likely formed the precipitate which contributed to the increasing pressure drop of the recirculating water loop filters and not the pump as initially theorized.

The incorporation of a mixed-resin DI bed in the recirculation loop will remove the acid degradation products as they are released by the membrane, thereby maintaining the pH of the loop somewhere between 5 and 6 as would be expected with a DI water loop in equilibrium with carbon dioxide from the cabin atmosphere. The pH in this range supports a 5-year life of the Hydrogen ORU. The DI bed will also scrub any cationic species that may be present due to low levels of corrosion of hardware in the recirculating water loop. The conductivity of the water will also decrease, reducing the shunt currents present between the cell stack anode and cathode.

Acknowledgments

The work described in this paper was performed by NASA, Boeing and Hamilton Sundstrand Space Systems International, Inc. (HSSSII) under the auspices of the International Space Station contract NAS15-10000. The authors wish to express their sincere thanks to Barbara Peyton, Carol Metselaar, Anne Dorazio and Robert Nowakowski of HSSSII Chemistry Lab; Kurt Critz and Michael O'Connor of the HSSSI Advanced Technology Lab; Elizabeth Bowman and the Boeing Huntsville Chemistry Lab; Al Pucino, Les Sinnock, Timothy Patterson, Thomas Skiba of UTC Power and T. T. Aindow, Chuck Burila, Bob Brown, Dan Goberman, Foster Lamm and Caitlyn Thorpe of the United Technologies Research Center.

References

Gray, F. M., *Polymer Electrolytes*, The Royal Society of Chemistry, 1997.

Davis, T. A., Genders, J. D., and Pletcher, D., *A First Course in Ion PermeableMembranes*, Alresford Press Ltd., 1997.

Barbir, F., *PEM Fuel Cells: Theory and Practice*, Elsevier Academic Press, 2005.

LaConti ,A. B., Fragala A. R., and Boyack J. R., "Solid Polymer Electrolyte Electrochemical Cell: Electrode and Other Materials Consideration", General Electric, *Proceedings of the Symposium on Electrode Materials and Processes for Energy Conversion and Storage*, The Electrochemical Society, Vol. 77(6), p. 314 (1977).

Okada, T.; Ayato, Y.; Yuasa, M.; Sekine, I. *J. Phys. Chem. B* **1999**, 103, 3315-3322.

Collier, A.; Wang, H.; Yuan, X.; Zhang, J.; Wilkinson, D. *International Journal of Hydrogen Energy 31* **2006**, 1838-1854.

Choudhury, B., *Material Challenges in Proton Exchange Membrane Fuel Cells*, Presentation at the International Symposium on Material Issues in a Hydrogen Economy, 2007.